

Nonperturbative and non-Markovian Förster-interaction in waveguiding systems

T. Sproll,¹ Ch. Martens,¹ M. P. Schneider,¹ F. Intravaia,^{1,2} and K. Busch^{1,2}

¹*Max-Born-Institut, 12489 Berlin, Germany*

²*Humboldt-Universität zu Berlin, Institut für Physik,
AG Theoretische Optik & Photonik, 12489 Berlin, Germany*

An exact solution to the interaction between two emitters mediated by Förster resonance energy transfer is presented. The system is comprised of a one-dimensional optical waveguide with two embedded two-level systems and is analyzed using a recently developed quantum-field theoretical approach. This exactly solvable model features several competing mechanisms that lead to a rich physical behavior such as, for instance, the possibility to change from an attractive to a repulsive interaction. Our nonperturbative analysis allows on very general grounds to describe the interaction as a truly non-Markovian phenomenon mediated by the atom-photon bound states of the system. These results are of direct relevance for energy or information transfer processes as well as for atom trapping more complex systems.

Since the seminal paper by T. Förster in 1948 [1], the field of nonradiative resonant energy transfer (FRET) has found wide-ranging applications in physics, chemistry and biology [2, 3]. In FRET, energy is exchanged between two emitters through nonradiative dipole-dipole interaction. This phenomenon is used to obtain information about signal transport inside biological systems [4] as well as to study the behavior and the interaction between proteins [5, 6]. Several methods of optical microscopy have used dimer-based FRET-induced fluorescence to circumvent the Abbé diffraction limit [7]. On another front, over the past decade, waveguide quantum electrodynamics (WQED) has attracted a growing attention [8–14]. In WQED systems, quantum emitters are coupled to an essentially one-dimensional electromagnetic environment, leading to interesting applications in the context of quantum information processing [15], also including the transport and storage of quantum information (often termed as the “Quantum Internet” [16]). Physical realizations at optical frequencies range from fibers with nearby trapped cold atoms [17] to photonic crystal waveguides with embedded emitters [18].

Here, we bring together these subjects of growing significance in physics and study their interplay. We show that for FRET in WQED systems, dispersion relation effects (e.g. slow light [8]) are of paramount importance. Specifically, at the level of the light-matter interaction, the peculiar behavior of the electromagnetic group-velocity, which under certain circumstances can be reduced to almost zero, introduces significant memory effects, carrying an intrinsic signature of non-Markovianity, which strongly modify the dynamic of the system. Probably the most unexpected manifestation of these phenomena is the appearance in the emitter’s dressing process of states, often termed atom-photon bound states (APBSs) [19]. Since these states drastically affect the nonradiative properties of the atom, they have a strong impact on the physics of the FRET mechanism. Our interest is twofold. First and contrary to many earlier investigations, the simplicity of our model system allows

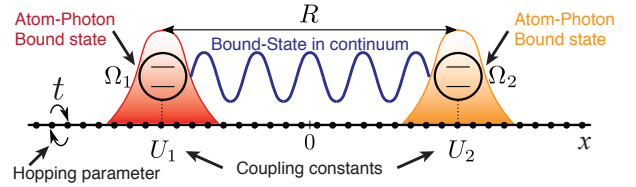


FIG. 1: (Color online) Schematic of the model system for studying FRET within WQED. Two TLSs with frequencies $\Omega_{1,2}$ coupled with strength $U_{1,2}$ to a waveguide with dispersion relation $\epsilon(k)$ and hopping parameter t .

to discuss FRET in a controlled environment, leading to a deeper understanding and to the highlighting of the relevant physical mechanisms. Second, FRET and related phenomena provide novel interesting effects and opportunities for WQED, such as additional communication channels and distinctive physical interactions mechanisms (e.g. trapping potentials).

Our system consists of a one-dimensional bosonic quantum wire formed by a chain of sites coupled to two two-level-systems (TLSs) separated by a distance R (measured in units of site spacing, see Fig. 1). To make the analysis of the underlying physical processes more transparent it is useful to describe each TLS within a slave fermion representation [1, 20]. Then, the Hamiltonian of our model system is given by ($\hbar = 1$)

$$\begin{aligned} \hat{H} = & \sum_k \epsilon(k) \hat{a}_k^\dagger \hat{a}_k + \sum_{j=1}^2 \frac{\Omega_j}{2} \left[\hat{f}_j^\dagger \{j\} \hat{f}_j \{j\} - \hat{g}_j^\dagger \{j\} \hat{g}_j \{j\} \right] \\ & + \sum_k \sum_{j=1}^2 \left[U_j e^{is(j)kR/2} \hat{a}_k^\dagger \hat{f}_j \{j\} \hat{g}_j^\dagger \{j\} + h.c. \right] \end{aligned} \quad (1)$$

Here, $\hat{a}_k^{(\dagger)}$ denotes photonic annihilation (creation) operators for the modes with wave number k of a waveguide with dispersion relation $\epsilon(k)$. Likewise, $\hat{f}_j^{(\dagger)}$ and $\hat{g}_j^{(\dagger)}$ represent fermionic annihilation (creation) operators corresponding to the ground (\hat{g}_j) and excited states (\hat{f}_j) of the two TLSs (labeled by $j = 1, 2$) with corresponding level

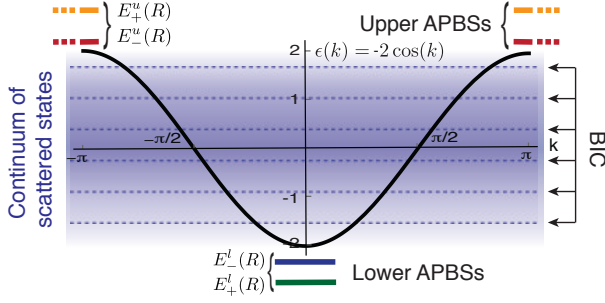


FIG. 2: (Color online) Energetic configuration for the Hamiltonian in Eq. (1) with $\epsilon(k) = -2 \cos(k)$ (the energies are normalized to the hopping parameter t ; see Fig. 1). The system's eigenenergies fall into three classes: a continuum of scattering states (shaded area), bound states in the continuum (BICs) [27] and atom-photon bound states (APBSs).

separations Ω_j . The constant U_j , describing the coupling strength of the TLSs to the waveguide can, without loss of generality, be assumed to be real and $s(j) = (-1)^j$ determines the sign in the Peierls factors [1]. In addition, we have employed the rotating wave approximation and the dipole approximation which is well-justified in the optical regime [22, 23]. For FRET, we can restrict ourselves to the one-excitation sector of the combined atom-photon Hilbert space. Here the (dressed) eigenstates of the Hamiltonian in Eq. (1) naturally separate into three classes (see Fig. 2). The first class corresponds to scattering states, which exhibit frequencies within the spectral bandwidth of the original waveguide. Bound states in the continuum (BIC) [24], characterized by discrete energies located within a dense continuum of scattering states form the second class. These BICs show up for identical atoms and correspond to the geometry-induced states of a perfect cavity where the two TLSs act as perfect mirrors [8, 25–27]. Finally, we have the third class of APBSs, whose eigenenergies are situated outside the spectrum of the waveguide [19] (see Fig. 2). They are characterized by wave functions that are exponentially localized around the locations of the TLSs [8]. APBSs only occur when the waveguide dispersion relation exhibits frequency cut-offs or band edges that are associated with slow-light regimes and non-Markovian dynamics [19, 28, 29]. The frequencies of the scattering states are insensitive to the separation of the TLSs and as the BIC states are embedded in a continuum, they induce only a small interaction between the TLSs which we shall neglect in subsequent discussion. Conversely, the number and properties of the APBSs strongly depend on the TLS separation R , inducing a significant nonradiative interaction between the emitters.

Using the properties of these states we can describe the waveguide-mediated interaction between the two TLSs

through the Förster potential defined as follows

$$\phi_{|\Psi\rangle}(R) = \sum_i [\alpha_{|\Psi\rangle,i}(R)E_i(R) - \alpha_{|\Psi\rangle,i}(\infty)E_i(\infty)]. \quad (2)$$

In Eq. (2), $E_i(R)$ denote the eigenenergies of the APBSs, $|\Psi\rangle$ is the state in which the system is initially prepared and $\alpha_{|\Psi\rangle,i} = |\langle\Psi|E_i\rangle|^2$ represent the eigenstate's occupation numbers. Within our model, the coefficients $\alpha_{|\Psi\rangle,i}$ play the same role as the orientation factors of ordinary three-dimensional FRET theory [1]. Notice that, due to the properties of the APBSs, the above expression can be regarded as a direct consequence of the non-Markovian dynamics of our system and loses its meaning as soon as these features disappear (e.g. for a linear waveguide dispersion relation, see below). Equation (2) reminds the definition of the Casimir energy [30] or, more specifically, its polaritonic contribution [31, 32]. Physically, it describes how the system's contribution to energy that stems from the APBSs, changes as a function of the distance between the TLSs. As for the Casimir effect, the $R \rightarrow \infty$ limit appearing in Eq. (2) sets the zero of the interaction potential to the configuration where the TLSs are well separated [33]. Note, however, that since in our case at least one of the TLSs is excited, we are dealing with an interaction that is similar to the van der Waals-Casimir-Polder potential of an excited atom near a surface [34–36] or near another atom [37–39].

In order to calculate $E_i(R)$ from the Hamiltonian (1), we employ and extend a Feynman diagram technique which has recently been developed and applied to the case of a single TLS [1] (see also [40]). The spectrum of a Hamiltonian can be obtained via the poles of the system's Green function [41]. In our subsequent calculations we focus on a cosine-shaped dispersion $\epsilon(k) = -2 \cos(k)$ which corresponds to a one-dimensional tight-binding chain with unit lattice spacing [28] (hereafter, all energies and frequencies are normalized to the hopping parameter, t in Fig. 1). This dispersion relation describes generic features such as band edges and slow-light regimes [8]. Both of them impact on the dynamics and the energy spectrum of the system, as it can be seen by inspecting first the self-energy $\Sigma_j(E) = -i\pi U_j^2 \rho(E)$ of an isolated TLS within a waveguide [1]. For a linear dispersion relation $\epsilon(k) \propto \chi v k$, with chirality χ and propagation speed v , the self-energy is constant since the density of states is $\rho(E) = 1/(\pi v)$. In this case, the Weisskopf-Wigner approximation [42] (equivalent to the Markov approximation [43]) holds exactly and the system undergoes a completely Markovian time evolution. In contrast, for the cosine-shaped dispersion relation the occurrence of a square-root singularity in the density of states $\rho(E) = i/[\pi\sqrt{E^2 - 4}]$ indicates a strongly non-Markovian behavior, especially for dynamics with energies located at borders of the waveguide energy-band, i.e. when $|E| \sim 2$. Physically, this can be understood

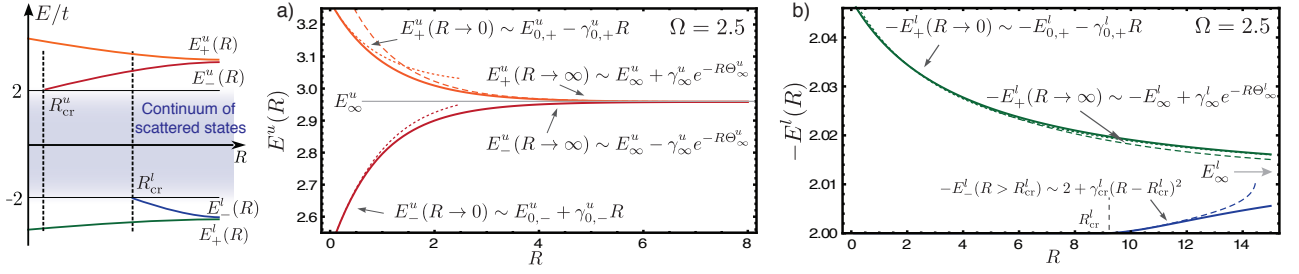


FIG. 3: (Color online) Eigenergies of the APBSs for a system with cosine-shaped dispersion relation. Left panel: A sketch of the typical behavior of the solutions of Eq. (5). Panels a) and b): Numerical solutions of Eq. (5) (full line) and the corresponding asymptotic calculations [44]. In both graphs, $E_{0,\pm}^{u,l} = 2 \cosh(\Theta_{0,\pm}^{u,l})$ and $E_{\infty}^{u,l} = 2 \cosh(\Theta_{\infty}^{u,l})$ denote the eigenvalues of Eq. (5) at $R = 0$ and $R = \infty$, respectively. We have introduced the quantities $\gamma_{0,\pm}^{u,l} = D(\Theta_{0,\pm}^{u,l})$ and $\gamma_{\infty}^{u,l} = D(\Theta_{\infty}^{u,l})$, where $D(\Theta) = U^2 \sinh(\Theta) / (2[\cosh(2\Theta) - \Omega \cosh(\Theta)])$, and $\gamma_{\text{cr}}^l = 4/(R_{\text{cr}}^l)^2$ [44]. Panel a): Energy values above the band ($E_{+,0}^u \approx 3.243$, $E_{-,0}^u \approx 2.544$, $E_{\infty}^u \approx 2.959$) with parameters $\Omega = 2.5$ and $U = 1$. Note that both curves stay finite for $R = 0$. Panel b): Negative of the energy values below the band ($E_{+,0}^l \approx -2.046$, $E_{\infty}^l \approx -2.012$) with the same parameters. The black line in panel b) indicates the critical value R_{cr} . See text for further details.

as resulting from the long atom-photon interaction times occurring in the slow light regimes and characterizing the system (memory-sensitive) time evolution [8].

An analogous but considerably richer behavior occurs in a system that contain two TLSs, which for simplicity, we take to be identical in the remainder of this work ($U_j = U, \Omega_j = \Omega$). Upon setting up the Feynman rules and summing up the resulting Dyson equation [1, 26, 44], we determine the Green's tensor of the system

$$\underline{\mathcal{G}}(R, E, k) = \underline{\mathcal{M}}(R, E, k) / Q(R, E). \quad (3)$$

In this expression $Q(R, E)$ is a scalar function (see also Eq. (4) below) and $\underline{\mathcal{M}}(R, E, k)$ is a second rank tensor which component-wise is analytic in R [44]. This means that all the nontrivial eigenenergies are determined by $Q(R, E) = 0$, which leads to the equation

$$(E - \Omega - \Sigma(E))^2 - \Gamma^2(R, E) = 0. \quad (4)$$

In this equation, $\Gamma(R, E) = U^2 \int G_w^0(k) e^{(-1)^s(j)ikR} dk$ represents a generalized self-energy ($\lim_{R \rightarrow 0} \Gamma(R, E) = \Sigma(E)$) and $G_w^0 = [E - \epsilon(k) + i0^+]^{-1}$ is the free-waveguide Green function. The eigenenergies $E_i(R)$ are real-valued solutions of Eq. (4) [27]. Since the APBSs' eigenenergies lie outside the photon continuum ($|E| > 2$), it is convenient to rewrite Eq. (4) as

$$2 \sinh(\Theta) (2 \cosh(\Theta) - \Omega) = U^2 (1 \pm e^{-\Theta R}), \quad (5)$$

where we have introduced the parametrization $\Theta(E) = \text{arccosh}(E/2) + \text{he}(-E)i\pi$, where $\text{he}(z)$ denotes the Heaviside function. In general, Eq. (5) features four distinct solutions: The \pm distinguishes the two solutions found above ($E_{\pm}^u > 2$) and the two solutions found below ($E_{\pm}^l < -2$) the cosine band (see Fig. 3 for their behavior and corresponding asymptotic expressions [44]). However, some of these solutions exist only if the condition

$$R > R_{\text{cr}}^{u,l} = 2(2 - \text{sign}(E^{u,l})|\Omega|)/U^2 > 0 \quad (6)$$

is fulfilled. Equation (6) indicates, that if R is larger than some critical value(s), one or, if $|\Omega| < 2$, even two (one below, for $R < R_{\text{cr}}^l$, and one above the band, for $R < R_{\text{cr}}^u$) of the four APBSs disappear into the waveguide continuum (see Fig. 3) [45]. This behavior can be viewed as consequence of the “level repulsion” occurring in the interacting system and giving rise to binding and anti-binding energetic configurations [31, 45]. The level repulsion increases for shorter distances and, depending on the value of E , one or even two of the four levels approach the band edge, eventually merging with the continuum of the scattering states at $R = R_{\text{cr}}^{u,l}$. Fig. 3 depicts the numerical solutions of Eq. (5) for $\Omega = 2.5$ and $U = 1$ as well as the corresponding asymptotic behaviors in the limits $R \rightarrow 0, R \approx R_{\text{cr}}^l$ (the only existing in this case) and $R \rightarrow \infty$. In agreement with Eq. (6), our analysis shows that one of the solutions below the band abruptly disappears in the continuum of scattering states and its behavior at $R \rightarrow R_{\text{cr}}^l$ is non-analytic in R . In fact for our model, as soon as the bound state reaches the band edge the associated wave function suddenly spreads over the entire waveguide, leading to a discontinuity in the derivative of the energy eigenvalue.

The last quantities required for calculating the FRET potential in Eq. (2) are the occupation numbers $\alpha_{|\Psi\rangle,i}$, which can be evaluated using resolvent theory [26, 44]. For the case of a initial state $|\Psi\rangle \equiv |1\rangle = |\uparrow, \downarrow, 0\rangle$, corresponding to one TLS being in the excited state (up arrow), the other TLS being in the ground state (down arrow) and zero photons in the waveguide we obtain [44]

$$\alpha_{|1\rangle,i}(R) = \text{Res}\{\mathcal{G}_{11}(R, E); E = E_i\}, \quad (7)$$

where the Green's function \mathcal{G}_{11} accounts for the propagation from the excited TLS back to itself including all scattering events. Upon inserting this information into Eq. (2), we obtain the Förster potential for two identical TLSs depicted in the inset of Fig. 4. As we consider

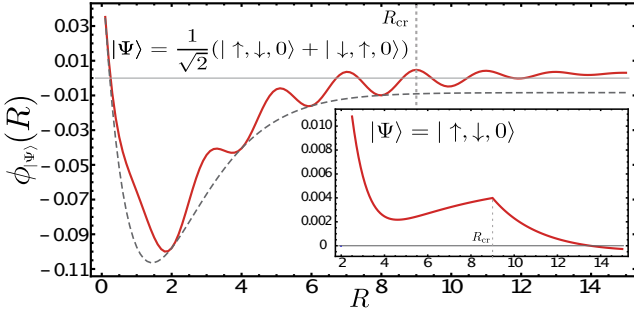


FIG. 4: (Color online) Förster potential $\phi_{|\Psi\rangle}(R)$ [Eq. (2)] as a function of the distance between two identical TLS ($\Omega = 2.5$) coupled to waveguide (coupling strength $U = 1$). For an initial state $|\Psi\rangle = (|\uparrow, \downarrow, 0\rangle + |\downarrow, \uparrow, 0\rangle)/\sqrt{2}$, $\phi_{|\Psi\rangle}(R)$ oscillates due to the change of parity of the APBS when changing R . It is dominated by contributions from eigenstates above the photon band (dashed line) while the oscillations come from contributions below the band. The Förster potential exhibits a global minimum at $R \approx 1.5$. Inset: For $|\Psi\rangle = |\uparrow, \downarrow, 0\rangle$, $\phi_{|\Psi\rangle}(R)$ shows a cusp due to the sudden emergence of a APBS from the continuum of scattering states.

transition frequencies Ω near the upper band edge, the contributions from the bound states above the band are much larger in magnitude and decay much faster with R than their counterparts from below the band. The contributions from below the band are negative and lead to a minimum in the potential $\phi_{|1\rangle}(R)$ which, for our choice of parameters, can be observed for $R \approx 4.5$. For $R = R_{\text{cr}}^l$, the emergence of one of the bound states from the continuum of the band leads to the sudden opening of a new nonradiative channel which creates a cusp in the Förster potential. For even larger values of R , $\phi_{|1\rangle}(R)$ becomes negative: This is due to the contribution of the added nonradiative channel which exceeds the contribution of others. As the Förster potential approaches zero for $R \rightarrow \infty$, this results in a shallow minimum (not shown in Fig. 4). To investigate the sensitivity of the potential to the initial state of the quantum system, it is interesting to calculate the Förster potential for the initial state $|\Psi\rangle \equiv |\pm\rangle = (|\uparrow, \downarrow, 0\rangle \pm |\downarrow, \uparrow, 0\rangle)/\sqrt{2}$ (we keep all other parameters the same). Proceeding as before, the corresponding occupation numbers above the band are

$$\alpha_{|\pm\rangle, i}^u(R) = \begin{cases} 2\text{Res}\{\mathcal{G}_{11}(R, E); E = E^u\} & \text{for } + \\ 0 & \text{for } - \end{cases} \quad (8)$$

This means that for the occupation to be nonzero the initial state must be symmetric with respect to the emitter's excitation, also implicitly revealing the symmetry of the APBSs above the band. Below the band, the situation is different. We obtain

$$\alpha_{|\pm\rangle, i}^l(R) = \text{Res}\{\mathcal{G}_{11}(R, E); E = E^l\} (1 \pm \cos(\pi R)), \quad (9)$$

showing that the occupation number oscillates on the length scale of the waveguide's site spacing. Indeed,

the photonic part of the wave function changes its parity if one TLS is kept fixed and another moved from a given site to the nearest neighbour site. The difference in the behavior of the states below or above the band can be traced back to the different degeneracies of the band edges within the Brillouin zone: The upper band edge occurs at the single point $k = \pm\pi$ in the Brillouin zone, whereas the lower band edge occurs at $k = 0$. The Förster potential corresponding to $|\Psi\rangle = |+\rangle$ is shown in Fig. 4. Due to the parity cancellation mechanism, we observe a minimum at $R \approx 1.5$ which is much deeper than in the case of $|\Psi\rangle = |1\rangle$. Furthermore, there is no cusp in the $\phi_{|+\rangle}(R)$ since it coincides with a zero in the occupation numbers given in Eq. (9). The oscillations we expect from Eq. (9) fade out for $R > R_{\text{cr}}^l$ due to destructive interference between the APBSs below the band edge. For the parameters we chose, the shifts $E_i^u(R) - E_i^u(\infty)$ above the band provide the dominating contribution to the potential (cf. Fig. 3).

In summary, we have analyzed in detail the FRET interaction between two TLSs mediated by the APBSs. The appearance of APBSs represents a non-Markovian effect which is a consequence of the boundedness of the waveguide spectrum. This behavior is absent in systems with unbounded dispersion relations, at least as long as the underlying rotating wave approximation is valid. Furthermore, we have demonstrated that the Förster potential can change from repulsive to attractive (featuring minima and maxima), depending on the distance between the TLSs. The Förster potential is also highly sensitive to the initial state of the system and we have compared two distinct initial states; in the first one, only one TLS is excited in the second one the excitation is distributed over the two TLSs in the form of an entangled state. While the latter yield a pronounced minimum, the former features a cusp due to the sudden emergence of an additional APBS from the continuum of scattering states. The structure of the Förster potential of our model is much richer than one would expect from the standard three-dimensional case, where the potential is monotonous and of the typical dipole-dipole form $\sim R^{-3}$ [1, 39]. This highlights the role of the electromagnetic environment which in our model is characterized by the bounded waveguide dispersion. The resulting novel features may lead to interesting applications. Firstly, the non-analytic behavior of $\phi_{|\Psi\rangle}(R)$ around R_{cr} facilitates the detection of a APBSs through suitably designed experiments. Secondly, the minima in the Förster potential can be used to trap atoms and/or nano-particles. Furthermore, it is quite conceivable to engineer a more interesting potential landscape by employing more than two TLSs, as additional APBSs will become available. In particular, this can be very interesting in the context of quantum simulations.

Acknowledgments. We acknowledge support by the Deutsche Forschungsgemeinschaft (DFG) through

project B10 within the Collaborative Research Center (CRC) 951 Hybrid Inorganic/Organic Systems for Opto-Electronics (HIOS). FI acknowledge support from the DFG via the DIP program (grant SCHM 1049/7-1).

-
- [1] T. Förster, *Annalen der Physik* **437**, 55 (1948).
- [2] R. B. Sekar and A. Periasamy, *J. Cell Biol.* **160**, 629 (2003).
- [3] S. Saini, H. Singh, and B. Bagchi, *J. Chem. Sci.* **118**, 23 (2006).
- [4] I. Endo and T. Nagamune, *Nano/Micro Biotechnology* (Springer, 2010).
- [5] B. A. Pollock and R. Heim, *Trends in Cell Biology* **9**, 57 (1999).
- [6] K. Truong and M. Ikura, *Current Opinion in Structural Biology* **11**, 573 (2001).
- [7] H. C. Ishikawa-Ankerhold, R. Ankerhold, and G. P. Drummen, *Molecules* **17**, 4047 (2012).
- [8] P. Longo, P. Schmitteckert, and K. Busch, *Phys. Rev. A* **83**, 063828 (2011).
- [9] H. Zheng and H. U. Baranger, *Phys. Rev. Lett.* **110**, 113601 (2013).
- [10] M. Laakso and M. Pletyukhov, *Phys. Rev. Lett.* **113**, 183601 (2014).
- [11] E. Shahmoon, I. Mazets, and G. Kurizki, *P.N.A.S.* (2014).
- [12] J. D. Hood *et al.*, *P.N.A.S.* **113**, 10507 (2016).
- [13] T. Shi, Y.-H. Wu, A. González-Tudela, and J. I. Cirac, *Phys. Rev. X* **6**, 021027 (2016).
- [14] P. Lodahl *et al.*, *Nature* **541**, 473 (2017).
- [15] T. D. Ladd, F. Jelezko, R. Laflamme, Y. Nakamura, C. Monroe, and J. L. O'Brien, *Nature* **464**, 45 (2010).
- [16] H. J. Kimble, *Nature* **453**, 1023 (2008).
- [17] D. Reitz, C. Sayrin, R. Mitsch, P. Schneeweiss, and A. Rauschenbeutel, *Phys. Rev. Lett.* **110**, 243603 (2013).
- [18] M. Arcari *et al.*, *Phys. Rev. Lett.* **113**, 093603 (2014).
- [19] S. John and J. Wang, *Phys. Rev. Lett.* **64**, 2418 (1990).
- [20] A. Auerbach, *Interacting Electrons and Quantum Magnetism* (Springer, 1994).
- [21] M. P. Schneider, T. Sproll, C. Stawiarski, P. Schmitteckert, and K. Busch, *Phys. Rev. A* **93**, 013828 (2016).
- [22] T. Mercouris, Y. Komninos, S. Dionissopoulou, and C. A. Nicolaides, *J. Phys. B: At. Mol. Opt. Phys.* **40**, 2133 (1997).
- [23] I. Feranchuk, I. I. Komarov, and A. P. Ulyanenko, *J. Phys. A: Math. Gen.* **29**, 4035 (1996).
- [24] F. H. Stillinger and D. R. Herrick, *Phys. Rev. A* **93**, 446 (1975).
- [25] G. Zumofen, N. M. Mojarad, V. Sandoghdar, and M. Agio, *Phys. Rev. Lett.* **101**, 180404 (2008).
- [26] T. Sproll, Ph.D. thesis, Humboldt-Universität zu Berlin, 2016.
- [27] For a general dispersion relation $\epsilon(k)$ and two identical emitters, one can show some real solutions of Eq. (4), which provides the eigenenergies of the Hamiltonian in Eq. (1), always occur for
- the atom-waveguide coupling physics parameters and are located within the continuum of the band energy spectrum (BIC). Although in Fig. 2 several BICs are represented, depending on the emitters' separation, only one state is selected by the system. Specifically, for the BIC obtained in the limit $R \rightarrow 0$ the system's dynamics shows some similarities with the behavior of the Dark States considered in C. Martens, P. Longo, and K. Busch, *New J. Phys.* **15**, 083019 (2013). Indeed, for $R \rightarrow 0$ in the one excitation sub-space our configuration turns out to be equivalent to a V-system. For non-identical TLSs, the cavity formed by the two emitters becomes leaky due to a mismatch in the individual mirror characteristics.
- [28] E. N. Economou, in *Green's functions in quantum physics, Solid-state sciences*, edited by M. Cardona, P. Fulde, K. von Klitzing, R. Merlin, and H.-J. Q. H. Störmer (Springer, Berlin / Heidelberg / New York, 2005).
- [29] Y. Liu and A. A. Houck, *Nat. Phys.* **13**, 48 (2017).
- [30] H. B. G. Casimir, *Proc. K. Ned. Akad. Wet.* **51**, 793 (1948).
- [31] F. Intravaia and A. Lambrecht, *Phys. Rev. Lett.* **94**, 110404 (2005).
- [32] F. Intravaia, C. Henkel, and A. Lambrecht, *Phys. Rev. A* **76**, 033820 (2007).
- [33] F. Intravaia and R. Behunin, *Phys. Rev. A* **86**, 062517 (2012).
- [34] J. M. Wylie and J. E. Sipe, *Phys. Rev. A* **32**, 2030 (1985).
- [35] F. Intravaia, C. Henkel, and M. Antezza, in *Casimir Physics*, Vol. 834 of *Lecture Notes in Physics*, edited by D. Dalvit, P. Milonni, D. Roberts, and F. da Rosa (Springer, Berlin / Heidelberg, 2011), pp. 345–391.
- [36] A. Laliotis, T. P. de Silans, I. Maurin, M. Ducloy, and D. Bloch, *Nat. Commun.* **5**, (2014).
- [37] H. R. Haakh, J. Schiefele, and C. Henkel, *Int. J. Mod. Phys.: Conf. Ser.* **14**, 347 (2012).
- [38] M. Donaire, R. Guérout, and A. Lambrecht, *Phys. Rev. Lett.* **115**, 033201 (2015).
- [39] P. W. Milonni and S. M. H. Rafsanjani, *Phys. Rev. A* **92**, 062711 (2015).
- [40] S. E. Kocabaş, *Phys. Rev. A* **93**, 033829 (2016).
- [41] G. D. Mahan, *Many-Particle Physics* (Springer, 2000).
- [42] V. Weisskopf and E. Wigner, *Z. Physik* **63**, 54 (1930).
- [43] P. R. Berman and G. W. Ford, in *Advances In Atomic, Molecular, and Optical Physics*, edited by E. Arimondo, P. R. Berman, and C. C. Lin (Academic Press, Amsterdam, 2010), Vol. 59, p. 175.
- [44] Supplemental Material at [URL will be inserted by publisher].
- [45] H. R. Haakh and F. Intravaia, *Phys. Rev. A* **88**, 052503 (2013).

$$E_{\text{BIC}} = \Omega = \epsilon \left(\frac{\pi N}{R} \right), \quad N \in \mathbb{Z}.$$

The solutions of the previous equation do not depend on

Supplemental Material

Nonperturbative and non-Markovian Förster-interaction in waveguiding systems

In this supplemental material we provide further details on the calculations leading to the results presented in the main text.

$$\underline{\mathcal{G}}(t', t) = -i \left\langle \begin{pmatrix} f^{\{1\}}(t) g^{\dagger\{1\}}(t) \\ f^{\{2\}}(t) g^{\dagger\{2\}}(t) \\ a_k(t) \end{pmatrix} \begin{pmatrix} f^{\dagger\{1\}}(t') g^{\{1\}}(t'), f^{\dagger\{2\}}(t') g^{\{2\}}(t'), a_{k'}^\dagger(t') \end{pmatrix} \right\rangle, \quad (\text{S1})$$

or equivalently in the frequency domain as

$$\underline{\mathcal{G}}(E) = \begin{pmatrix} \mathcal{G}_{11} & \mathcal{G}_{21} & \mathcal{G}_{\text{ph},1} \\ \mathcal{G}_{12} & \mathcal{G}_{22} & \mathcal{G}_{\text{ph},2} \\ \mathcal{G}_{1,\text{ph}} & \mathcal{G}_{2,\text{ph}} & \mathcal{G}_w \end{pmatrix}. \quad (\text{S2})$$

The Green functions with numbered indices appearing as elements of the above matrix describe an excitation moving from one TLS to another one (or staying at the same TLS), \mathcal{G}_w describes photons in the waveguide - renormalized by interaction with both TLS - and the other Green functions describe absorption and emission processes.

The form of the Green tensor in Eq. (3) of the main text derives from the observation that, due to the Peierls substitution, the R -dependence in the perturbation series is totally encapsulated in the one-photon loop diagram (equivalent to the total system's self-energy) up to a possible phase factor due to external legs of the diagram. Its 3×3 matrix structure is a consequence of the scattering processes (channels) characterizing our system in the one-photon sector. (See also the amputation rules for Feynman diagrams discussed in context of waveguide QED in Ref. [1].) As an example of the calculation, we consider the Green's function \mathcal{G}_{11} . The corresponding Dyson equation reads

$$\mathcal{G}_{11}(R) = G_1 + (U_1 U_2)^2 \Gamma(R) G_1 \Gamma(R) G_2 \mathcal{G}_{11}(R), \quad (\text{S3})$$

where, for reasons of a compact notation, we have suppressed the argument E . This is equivalent to

$$\mathcal{G}_{11}(R) = \frac{G_1}{1 - (U_1 U_2)^2 \Gamma(R)^2 G_2 G_1} \equiv \frac{[\mathcal{M}(R)]_{11}}{Q(R)}, \quad (\text{S4})$$

where G_1 and G_2 are the, R -independent, one-scatterer renormalized Green functions [1]. We observe that the R -dependent self-energy, $\Gamma(R)$ as given in the main text, does not depend on k , since the photon momentum is

The Green function of the system can be written as the ordered dyadic product of vectors containing the creation and the annihilation (bosonic and fermionic) operators involved in the system (see the main text after Eq. (1)). In the Heisenberg picture we have

integrated out. This explains the factorization mentioned in the main text.

The same Green tensor formalism can be used to extract the occupation numbers $\alpha_{|\Psi\rangle,i} = |\langle\Psi|E_i\rangle|^2$. Together with the eigenenergies, they are one of the two main elements involved in the definition of the Förster potential in Eq. (2) of the main text.

We start by noticing that to each Green tensor we can associate a quantum operator. For example the waveguide (w) Green function denoted by \mathcal{G}_w is given in Heisenberg representation by $\mathcal{G}_w = \langle 0 | a_k a_k^\dagger | 0 \rangle$ (cf. Eqs. (S1) and (S2)) and we can identify $\hat{G}_w = \hat{a}_k \hat{a}_k^\dagger$ as the corresponding quantum operator. In general, it is convenient to express this operator using a spectral decomposition (often called Lehmann representation in many-body theory [2])

$$\hat{G}(E) = \sum_i \frac{|E_i\rangle\langle E_i|}{E - E_i}, \quad (\text{S5})$$

where $\{|E_i\rangle\}$ corresponds to the energy eigenbasis. For a general state $|\Psi\rangle$ we then have

$$\langle\Psi|\hat{G}(E)|\Psi\rangle = \sum_i \frac{|\langle\Psi|E_i\rangle|^2}{E - E_i}. \quad (\text{S6})$$

Invoking the residue theorem and integrating around a closed contour which contains exactly one eigenvalue, we have

$$\text{Res}(\langle\Psi|\hat{G}(E)|\Psi\rangle, E = E_i) = |\langle\Psi|E_i\rangle|^2 \equiv \alpha_{|\Psi\rangle,i}. \quad (\text{S7})$$

Let us apply the above general considerations to one of the configurations analyzed in the main text. Consider a system of a waveguide coupled to two TLSs, one of which is excited, i.e. $|\Psi\rangle = |1\rangle = |\uparrow, \downarrow, 0\rangle$. In this case the relevant Green tensor is $\langle 1 | \hat{G}(E) | 1 \rangle = \mathcal{G}_{11}(R, E)$, which

is the Green function already defined in Eq.(S4). This means

$$\alpha_{|1\rangle,i} = \text{Res}\{\mathcal{G}_{11}(E), E = E_i\}, \quad (\text{S8})$$

where E_i are the solutions for $|E_i| > 2$ of Eq. (4) of the main text.

Asymptotic expressions for the APBSs energies

In following section we want to motivate the asymptotic values for the eigenenergies of the system given in Fig. 6 of the main text. We employ the parametrization $\Theta = \text{arccosh}(E/2)$ as described in the main text and for simplicity let us define

$$f(\Theta) = \sinh(2\Theta) - \Omega \sinh(\Theta) - \frac{U^2}{2}, \quad (\text{S9})$$

focusing on the regime $E^u > 2$ removing the corresponding superscript. The values below the band (E_{\pm}^l) can be obtained by making the replacement $R \rightarrow -R$ and $\Omega \rightarrow -\Omega$ in all following equations. For $R\Theta_{0,\pm} \ll 1$, where $\Theta_{0,\pm}$ are the values corresponding to $E_{\pm}(R \rightarrow 0)$, we write $\Theta = \Theta_{0,\pm} + \delta_{0,\pm}(R)$ with $\delta/\Theta_0 \ll 1$ and get from Eq. (5) in the main text:

$$\delta_{0,\pm}(R) \approx \mp \frac{U^2}{2} \frac{R\Theta_{0,\pm}}{2 \cosh(2\Theta_{0,\pm}) - 2\Omega \cosh(\Theta_{0,\pm})}, \quad (\text{S10})$$

where we have neglected terms of order $R\delta(R)$, since they turn out to be of order $\mathcal{O}(R^2)$. Expanding $E_{\pm} = 2 \cosh(\Theta_{0,\pm} + \delta_{0,\pm}(R))$ up to first order we have

$$E_{\pm} \sim 2 \cosh(\Theta_{0,\pm}) \mp \gamma_{0,\pm} R, \quad (\text{S11})$$

which are the expressions that are reported in the plots of Fig. 3 of the main text. For brevity, we have defined the term $\gamma_{0,\pm} = \sinh(\Theta_{0,\pm})U^2/f'(\Theta_{0,\pm})$ (the prime denotes a derivative with respect to the argument).

We use a similar approach for the opposite limit $\Theta_{\infty,\pm}R \gg 1$, where $\Theta_{\infty,\pm}$ corresponds to the eigenenergy $E_{\pm}(R \rightarrow \infty)$. Solving self-consistently Eq. (5) of the main text, we obtain

$$\delta_{\infty,\pm}(R) \sim \pm \frac{U^2 e^{-\Theta_{\infty} R}}{f'(\Theta_{\infty})} \quad (\text{S12})$$

(in this case $\exp(-\Theta R)/2 \ll 1$ is the small quantity relevant for the expansion). This yields

$$E_{\pm} \sim 2 \cosh(\Theta_{\infty}) \pm \underbrace{\frac{\sinh(\Theta_{\infty})U^2}{f'(\Theta_{\infty})}}_{=\gamma_{\infty}} e^{-R\Theta_{\infty}}, \quad (\text{S13})$$

which, again, are the expressions that are reported in Fig. 3 of the main text. Equation (S13) shows how the

energies become degenerate for large separations while they progressively split (level repulsion) as the TLSs get closer.

Finally, for $R \approx R_{\text{cr}}$ we might perform an expansion in $\Delta R = R - R_{\text{cr}}$, obtaining ($\Delta R/R_{\text{cr}} \ll 1$)

$$\Delta R - \Theta \frac{R^2}{2} \approx 0, \quad (\text{S14})$$

which and after some simple algebra leads to the result stated in the main text, i.e.

$$E \sim 2 + \underbrace{\frac{4}{R_{\text{cr}}^2}}_{\gamma_{\text{cr}}} (\Delta R)^2. \quad (\text{S15})$$

Notice that the case where $R_{\text{cr}} \rightarrow 0$ features additional complications that require a higher-order expansion resulting in

$$E \approx 2 + \frac{U\sqrt{3\Delta R}}{\sqrt{8-\Omega}}. \quad (\text{S16})$$

T. Sproll¹, Ch. Martens¹, M. P. Schneider¹, F. Intravaia^{1,2} and K. Busch^{1,2}.

¹ Max-Born-Institut, 12489 Berlin, Germany

² Humboldt-Universität zu Berlin, Institut für Physik, AG Theoretische Optik & Photonik, 12489 Berlin, Germany

-
- [1] M. P. Schneider, T. Sproll, C. Stawiarski, P. Schmitteckert, and K. Busch, "Green's-function formalism for waveguide QED applications", Phys. Rev. A **93**, 013828 (2016).
 - [2] H. Bruus and K. Flensburg, *Many-body quantum theory in condensed matter physics* (Oxford University Press Oxford, New York, 2004).